Available online at www.sciencedirect.com
SCIENCE DIRECT®
Journal of Solid State Chemistry 177 (2004) 3918–3926
JOURNAL OF SOLID STATE CHEMISTRY
www.elsevier.com/locate/jssc

Strong anisotropic thermal expansion in cristobalite-type BPO_4

S.N. Achary, A.K. Tyagi*

Applied Chemistry Division, Solid State Chemistry Section, Bhabha Atomic Research Centre, Mumbai 400 085, Maharashtra, India

Received 12 May 2004; received in revised form 29 June 2004; accepted 9 July 2004
Available online 18 September 2004

Abstract

In this communication, the thermal expansion behavior of cristobalite-type BPO_4, determined from high-temperature X-ray diffraction studies, is being reported. BPO_4 crystallizes in tetragonal lattice, with space group $I\bar{4}$ (No. 82) at room temperature, with unit cell parameters: $a=4.3447(2)$, $c=6.6415(5)$ Å and $V=125.37(1)$ Å^3. The tetragonal unit cell parameters at 900 °C are: $a=4.3939(2)$, $c=6.6539(6)$ Å and $V=128.46(1)$ Å^3. The results show a very strong anisotropic expansion in the lattice, with the typical thermal expansion coefficients along a- and c-axis 12.9×10^{-6} and 2.1×10^{-6}/°C, respectively. The volume thermal expansion coefficient of the lattice is 28.2×10^{-6}/°C in the temperature range of 25–900 °C. The variation of the crystal structure with temperature and the thermal expansion behavior are explained in this manuscript. The role of inter-polyhedral angle on the thermal expansion behavior has also been established.

Keywords: Thermal expansion; Cristobalite; Phosphates; HT-XRD

1. Introduction

Thermal expansion is an important property generally considered for the construction of high-temperature ceramic devices. In this aspect, the materials with negative or low thermal expansion are desired to act as a buffer for temperature-induced stress on a material due to another component of structural materials. It is well known that thermal expansion of a chemical bond arises from the anharmonicity in the potential energy curves. The mean bond length increases due to the increase in the amplitude of vibration of the atoms with temperature, which is reflected in the expansion of the material. However, there are several groups of materials where instead of an expansion behavior, anomalous expansions like, low or negative expansion are observed. The anharmonicity concept fails to explain the unusual thermal expansion of such materials. The crystal structures of such a group of materials provide an explanation for this unusual thermal expansion behavior. Sleight and co-workers [1–8] have studied a large group of framework materials in phosphates, tungstates, molybdates, etc. and arrived at a close correlation between the structure and anomalous expansion. From these studies it is well understood that the transverse vibration of bridging atoms of framework crystals causes negative or low thermal expansion [1,5]. All these thermal expansion characteristics were explained on the basis of variation of M–O–M' bond angles, as a function of temperature due to the tilting of polyhedra. In addition, the packing density of the lattice also plays an important role in the lattice expansion [4]. The strong covalency of the chemical bonds in general leads to rigid polyhedral units and tilting of such polyhedra often leads to anomalous expansion behavior [6–9]. A general survey of crystal structures of these kind of materials indicates that the lower packing density and flexible structures formed by connecting the polyhedral units only at the corners seem to be the common features among the materials showing negative thermal

*Corresponding author. Fax: +91-22-2550-5151.
E-mail addresses: sachary@apsara.barc.ernet.in (S.N. Achary), aktyagi@magnum.barc.ernet.in (A.K. Tyagi).

0022-4596/$ - see front matter © 2004 Elsevier Inc. All rights reserved.
doi:10.1016/j.jssc.2004.07.036

expansion behavior [4,8,9]. Such structures allow low energy vibration modes and hence exhibit anomalous thermal expansion [10,11]. Therefore, the search for materials with such anomalous expansion, namely anisotropic, low or negative thermal expansion is mainly focused in flexible low-density framework-type crystal structures [1–9].

Recently, we have studied the thermal expansion characteristics of a series of cristobalite-type phosphates ($Al_{1-x}Ga_xPO_4$; $0.0 \leqslant x \leqslant 1.0$), where a close relation of inter-polyhedral angle (M–O–P) and thermal expansion is concluded [9]. In all these studied phosphates, the transformation of the low-cristobalite to high-cristobalite phase is accompanied with a significant rise in the unit cell volume. The high-cristobalite phase has a significantly lower thermal expansion compared to the low-temperature (low-cristobalite) phase. In the present study, a similar high-cristobalite framework-type phosphate BPO_4 is studied by high-temperature X-ray diffraction (HT-XRD) in order to further investigate the role of inter-polyhedral angle on thermal expansion behavior. BPO_4 crystallizes in tetragonal lattice similar to the high-cristobalite-type structure [12] as well as in quartz-type structure under high-pressure and high-temperature conditions [13,14]. The quartz-type BPO_4 can be retained at ambient temperature by quenching from high-temperature and high-pressure conditions [13,14]. Besides, there is no low-cristobalite analog structure reported for this compound. In both cristobalite- or quartz-type BPO_4 structures, the BO_4 and PO_4 tetrahedral units share corners forming the three-dimensional lattice.

The tetragonal structure of high-cristobalite-type BPO_4 is formed due to the tilting of the tetrahedra about the two-fold axis parallel to c-axis in C9 structure [15,16]. All the silica analog compounds have been of interest due to their structural flexibility under pressure and/or temperature. On application of pressure the polyhedra in framework-structured compounds rearrange to give denser meta-stable structures either by displacive or reconstructive transitions [17,18]. Similarly, the temperature-induced structural transformations are also known for this class of compounds [19,20]. Recently, the variation of crystal structure of BPO_4 with pressure has been reported, which indicates an increase in tilting angle with increasing pressure [21] and finally leads to collapsing of the framework structure to a structure with denser cubic close packing of oxygen atoms. In general, the temperature and pressure have a competing relation in crystalline materials. Hence, to study the structural variation with temperature and to observe the thermal expansion characteristics, the present study was carried out and the results are described. Also, the thermal expansion characteristic of BPO_4 is compared with other analogous cristobalite-type compounds.

2. Experimental

Stoichiometric amounts of di-ammonium hydrogen phosphate ($(NH_4)_2HPO_4$) and boric acid (H_3BO_3) were dissolved in distilled water. The clear solution was obtained after warming the solution. The effervescence from the solution was removed by carefully shaking the container. The solution was gently evaporated on a hot plate. The gelly mass obtained was further dried on hot plate, till it got converted to a dry powder. The powder sample was further heated at 800 °C for 15 h in a platinum boat. The product obtained was characterized by power XRD patterns recorded on a Philips PW1710 model powder X-ray diffractometer, using Cu$K\alpha$ radiation. The XRD patterns of the samples at higher temperatures were recorded on a Philips X-Pert Pro diffractometer, with Anton Parr high-temperature attachment. The well ground sample was mounted on a platinum strip, which served the purpose of both sample holder as well as heater. The XRD patterns were recorded in the 2θ range of 20–80 °C with step and step time as 0.02° and 1.6 s, respectively. The diffracted beam is monochromatized using a curved graphite monochromator. The sample was heated to a desired temperature at the rate of 20 °C/min and held for 5 min for equilibration and then XRD data were collected. The temperature was controlled with Eurotherm temperature programmer, with an accuracy of ± 1 °C.

3. Results and discussion

The phase purity of the prepared BPO_4 sample was inferred by comparing the observed powder XRD pattern with the reported JC-PDS data 34-0132. The further characterization of the sample was carried out by the Rietveld refinement of the observed powder diffraction profile using Fullprof software package [22]. The starting model for the refinement of room temperature phase was taken from the reported structure of BPO_4 (P: 2a; B: 2c and O: 8g (x, y, z), $Z = 2$ and space group I-4, No. 82) [12]. It needs to be mentioned here that since the platinum strip was used as the sample holder, the reflections due to this also appeared in the observed data. Hence, a biphasic refinement was carried out. Initially, the scale, background and unit cell parameters were refined for both the phases together. The profile was fitted using pseudo-Voigt profile function. The typical half-width, mixing parameters, preferred orientation and the asymmetry parameters were also refined. The preferred orientation was modeled by March function provided in the Fullprof software. Subsequently, the position coordinates of oxygen atoms were refined and then the isotropic thermal parameters of all the atoms were

refined independently. In general, PO_4 and BO_4 groups are known to act as a rigid polyhedra, as the P–O and B–O bonds do not show any variation with temperature, as observed in the literature [9,23]. In addition, due to the low scattering factor of B and similar scattering factor of O and P, soft bond constraints with 1.47 and 1.52 Å for the B–O and P–O, respectively, were used in the refinements. The magnitudes of the constraints are 0.025 Å for these two bonds. The goodness of the refinement was observed from the residuals (R-values) of the refinements.

The refined unit cell parameters for BPO_4 at ambient temperature are $a=4.3447(2)$, $c=6.6415(5)$ Å, $V=125.37(1)$ Å^3 ($R_p=13.6$, $R_{wp}=19.6$, $\chi^2=1.8$ and $R_B=1.6$), which are in good agreement with the reported data [12,21]. The typical observed and calculated XRD patterns along with the difference plot are shown in Fig. 1. The crystal structure of BPO_4 is built by sharing the corner of BO_4 and PO_4 tetrahedra leading to a framework structure. Thus, each oxygen atom has a coordination number of two (one P and B atom each) in the lattice. A typical three-dimensional representation of typical BPO_4 structure is shown in Fig. 2. The other details of the crystallographic parameters of this phase are summarized in Table 1.

The observed XRD profiles at higher temperature were refined in a similar fashion, with the starting model taken from the refined parameters of pervious temperature data. The refined unit cell parameters of BPO_4 at 900 °C are $a=4.3939(2)$, $c=6.6539(6)$ Å and $V=128.46(1)$ Å^3 (space group $I\bar{4}$, No. 82 and $R_p=15.6$, $R_{wp}=21.2$, $\chi^2=2.3$ and $R_B=2.1$). The observed and the calculated diffraction profiles along with the difference plot for BPO_4 at 900 °C are shown in Fig. 3. The refined parameters and other details for BPO_4 at various temperatures are given in Table 1. The typical

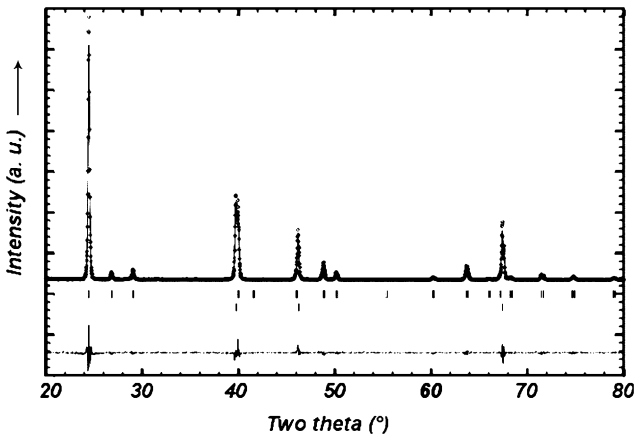

Fig. 1. Observed and calculated XRD patterns of BPO_4 at 25 °C: vertical marks indicate the Bragg positions and lower vertical marks indicate platinum base metal reflections. $U=0.33(5)$, $V=-0.20(4)$, $W=0.07(1)$, $\eta=0.30(1)$, $A1=0.070(6)$, $A2=0.010(2)$ and preferred orientation = 0.975(9) (vector = [001] and March model).

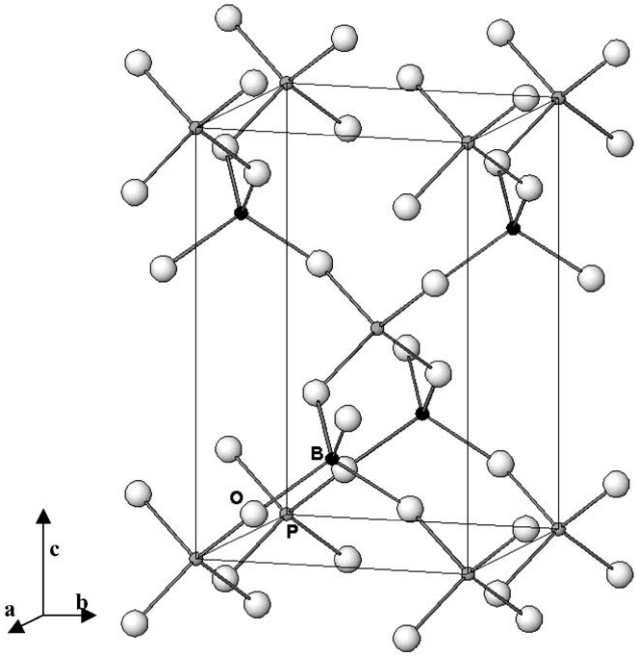

Fig. 2. Crystal structure of BPO_4 at room temperature (25 °C).

B–O and P–O bond lengths and the B–O–P bond angles at various temperatures are given in Table 2. The observed separations of B and P atoms are also given in Table 2. The variation of unit cell parameters with temperature is shown in Figs. 4 and 5. It is observed that the a- and b-axis expand significantly compared to the c-axis. The typical thermal expansion coefficients, in the temperature range of 25–900 °C, along a- and c-axis are 12.9×10^{-6} and 2.1×10^{-6}/°C, respectively. The volume thermal expansion coefficient of the lattice is 28.2×10^{-6}/°C, in the temperature range of 25–900 °C.

The cristobalite forms of $AlPO_4$ and $GaPO_4$ are known to transform [9] from orthorhombic to cubic modification at higher temperature. It is also reported that cubic high-cristobalite phase has considerably lower thermal expansion than the orthorhombic phase. The thermal expansions of low-cristobalite-type $AlPO_4$ and $GaPO_4$ (orthorhombic, C2221) have only a small anisotropy along various axes [9]. But in the present case a strong anisotropy is observed along a- and c-axis. Thus, the c/a value changes from 1.53 to 1.51 as the temperature increases from 25 to 900 °C. For the ideal cristobalite-type cubic compounds namely SiO_2, $AlPO_4$ and $GaPO_4$ the c/a value is 1.414 (i.e., $\sqrt{2}$) (in an equivalent tetragonal lattice). The c/a values at other temperatures are also included in Table 2. A comparison of the variation of c/a with temperature and the reported data on variation of c/a with pressure [21] indicates an inverse relation of pressure and temperature, i.e., on application of pressure the c/a increases as against the decrease with temperature.

Table 1
Typical unit cell parameters of BPO_4 at various temperatures

Temp. (°C)	a (Å)	c (Å)	V (Å^3)	Oxygen position coordinates[a]			(B) B (Å^2)	(P) B (Å^2)	(O) B (Å^2)	R_p, R_{wp} χ^2 and R_B
				x	y	z				
25	4.3447(2)	6.6415(5)	125.37(2)	0.1389(10)	0.2589(11)	0.1275(5)	2.9(6)	2.4(1)	3.7(2)	13.6,19.6,1.8, 1.6
100	4.3475(2)	6.6416(5)	125.53(1)	0.1393(9)	0.2574(11)	0.1275(5)	3.7(6)	2.6(1)	3.6(2)	12.8,18.7, 1.6,1.6
200	4.3522(2)	6.6424(5)	125.82(1)	0.1374(10)	0.2578(11)	0.1270(5)	3.4(6)	2.9(1)	3.6(2)	13.1,19.4,1.7,1.4
300	4.3579(2)	6.6426(5)	126.15(1)	0.1369(10)	0.2566(11)	0.1261(5)	3.0(6)	2.9(1)	4.0(2)	13.6,14.6,1.8,1.7
400	4.3632(2)	6.6445(5)	126.50(1)	0.1353(10)	0.2566(11)	0.1264(6)	2.9(6)	3.1(1)	4.0(2)	13.8,18.2,2.0, 1.6
500	4.3686(2)	6.6466(5)	126.85(1)	0.1336(11)	0.2569(12)	0.1259(6)	2.9(6)	3.2(2)	4.2(2)	17.9,23.1, 2.0,2.2
600	4.3749(2)	6.6477(5)	127.23(1)	0.1325(11)	0.2563(12)	0.1254(6)	2.6(6)	3.2(2)	4.5(2)	13.6,19.1, 2.4,1.5
700	4.3808(2)	6.6499(5)	127.62(1)	0.1316(11)	0.2574(12)	0.1255(6)	2.7(7)	3.4(2)	4.5(2)	14.7,20.5,2.1,1.8
800	4.3876(2)	6.6521(5)	128.06(1)	0.1302(11)	0.2565(12)	0.1252(6)	2.8(7)	3.3(2)	5.0(3)	15.0, 20.4, 2.1, 2.2
900	4.3939(2)	6.6539(6)	128.46(1)	0.1274(12)	0.2569(13)	0.1250(7)	3.2(7)	3.6(2)	5.2(3)	15.6,21.2,2.3,2.1

[a]O: 8g (x, y, z), B: 2c (0, $\frac{1}{2}$, $\frac{1}{4}$) and P: 2a (0, 0, 0) (space group I-4, No. 82 and $Z = 2$). Oxygen parameters for ideal C9 structure (0, 0.25, 0.125).

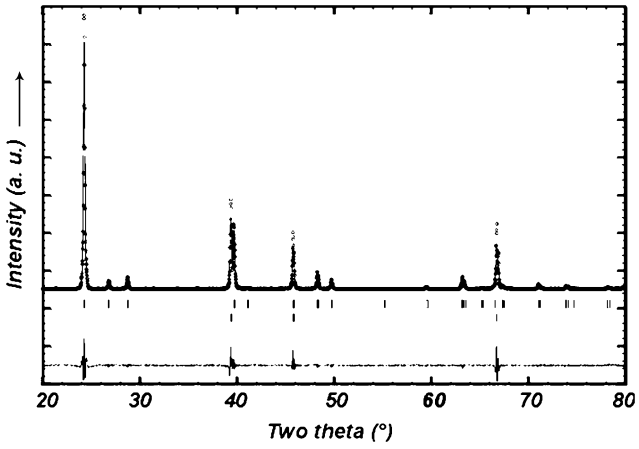

Fig. 3. Observed and calculated XRD patterns of BPO_4 at 900 °C: vertical marks indicate the Bragg positions and lower vertical marks indicate platinum base metal reflections. $U = 0.14(3)$, $V = -0.15(2)$, $W = 0.056(4)$, $\eta = 0.41(1)$, $A1 = 0.022(7)$, $A2 = -0.002(3)$ and preferred orientation = 1.00(1) (vector = [001] and March model).

Table 2
Typical bond lengths and bond angles and tilt angles in BPO_4 at various temperatures

Temp. (°C)	B–O (Å)	P–O (Å)	P···B (Å)	P–O–B (°)	Tilt angle (°)[a]	c/a
25	1.458(4)	1.532(4)	2.7342(1)	132.33(29)	29.06	1.529
100	1.463(4)	1.528(4)	2.7353(1)	132.22(29)	29.13	1.528
200	1.462(4)	1.526(4)	2.7373(1)	132.76(29)	28.79	1.526
300	1.470(4)	1.519(4)	2.7396(1)	132.92(30)	28.71	1.524
400	1.467(4)	1.519(4)	2.7420(1)	133.37(30)	28.42	1.523
500	1.466(5)	1.516(5)	2.7445(1)	133.89(33)	28.12	1.521
600	1.469(5)	1.513(5)	2.7471(1)	134.21(33)	27.92	1.520
700	1.466(5)	1.516(5)	2.7499(1)	134.47(34)	27.76	1.518
800	1.469(5)	1.512(5)	2.7529(1)	134.89(36)	27.51	1.516
900	1.465(5)	1.509(5)	2.7557(1)	135.76(39)	27.00	1.514

[a]Tilt angle $\phi = \tan^{-1}(4x)$, where $x = x$ coordinates of oxygen position.

The typical thermal expansion characteristics of some cristobalite-type compounds are also included in Table 3, for comparison. The variations of various

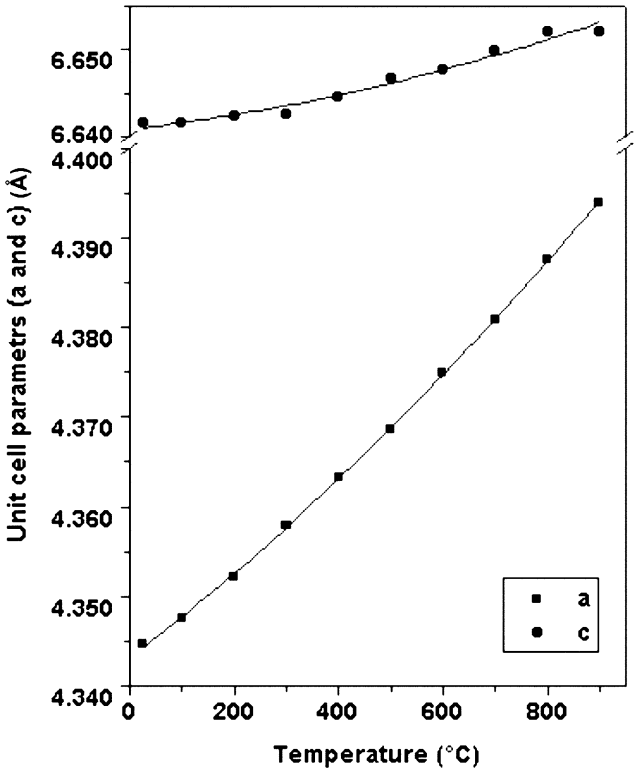

Fig. 4. Variation of unit cell parameters (a and c) with temperature (accuracy: ±0.0005 and ±0.0012 Å for a and c, respectively). The error bars are smaller than the symbol size.

inter-atomic separations with temperature are shown in Fig. 6. From this figure, it is clear that typical B–O bond does not show appreciable change with temperature. However, it is observed that there is a subtle but noticeable decrease in P–O bond length with temperature. Such decrease in bond length is only apparent and results from the thermal vibration of the connecting oxygen atoms. Similar apparent decrease in bond length with temperature is observed in several framework compounds like orthorhombic-$NbOPO_4$ [4], $Y_2(WO_4)_3$ [5] and $Sc_2(WO_4)_3$ [8]. This apparent decrease in bond

length is explained as an effect of the thermal motion of the oxygen atoms [4–5,8,24,25]. The variable temperature structural data for SiO_2 (quartz) also show a similar decrease in Si–O bond length with temperature, even though the total neutron scattering (considering both the Bragg and diffuse scattering) data show a small increase in Si–O bond [26]. Grimm and Dorner [27] have earlier suggested the thermal contraction of the Si–O bond in quartz is due to the increase of the π-bond order with the increase of Si–O–Si bond angles. However, later studies in various framework-type phosphates, tungstates or silicates support the origin of the bond shortening due to the elliptical nature of the vibration amplitude of the connecting atoms [4–5,8,24–26,28]. As the amplitude of the thermal vibration of the bridging oxygen increases with increase of temperature such deviations are expected. The variations of the isotropic thermal parameters for various atoms are shown with temperature in Fig. 7 and Table 1. It is evident that the mean amplitude of vibration of B does not show much deviation compared to P. But the mean amplitude of vibration of oxygen atoms increases significantly with increasing temperature. Thus, the increasing thermal motions of oxygen atoms are resulted in the shortening of the P–O bond. This suggests that the observed

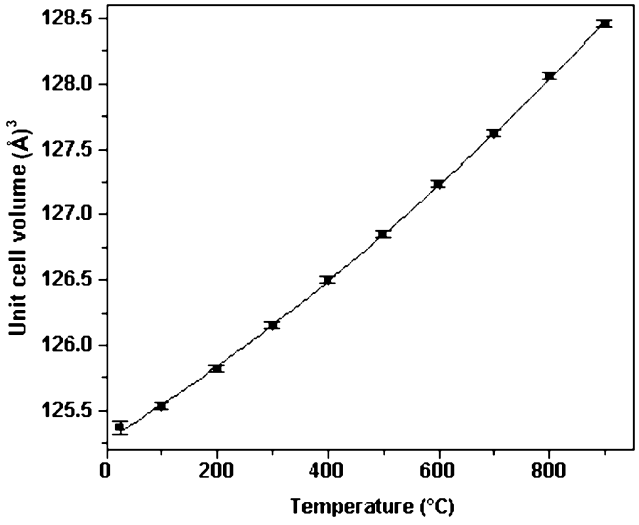

Fig. 5. Variation of unit cell volume with temperature, V (Å)$^3 = 125.276 + 0.003[T] + 1.043 \times 10^{-6}[T]^2$.

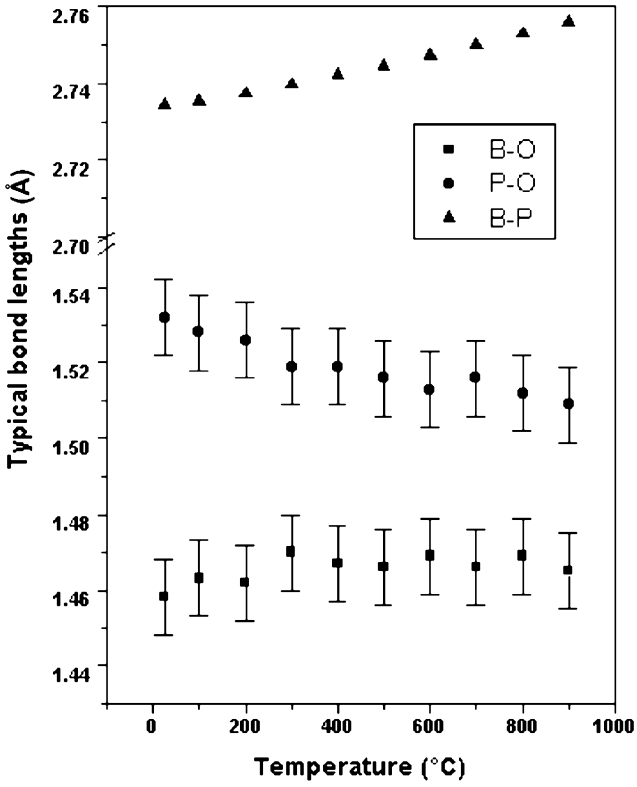

Fig. 6. Variation of typical inter-atomic distances with temperature. Accuracy for B–P distances is ±0.0002 Å. The error bars are smaller than the symbol size.

Table 3
Thermal expansion coefficient of BPO_4, for comparison typical thermal expansion coefficients of other cristobalite-type compounds are given

	Temp. range (°C)	Crystal symbol	$\alpha_a \times 10^6$/°C	$\alpha_b \times 10^6$/°C	$\alpha_c \times 10^6$/°C	$\alpha_V \times 10^6$/°C
BPO_4	25–900	T	2.1	—	12.9	28.2 (present data)
$AlPO_4$	25–200	O	27.4	27.2	44.5	99.8 [9]
	300–1000	C	1.93	—	—	5.75 [9]
	25–1000*	—	—	—	—	67.5 [9]
	300–1000	C	2.02			6.08 [30]
$Al_{0.5}Ga_{0.5}PO_4$	25–300	O	18.7	22.4	30.4	71.9 [9]
	400–1000	C	5.52	—	—	16.6 [9]
	25–1000*	—	—	—	—	86.1 [9]
$GaPO_4$	25–600	O	18.5	19.8	23.2	62.2 [9]
	700–1000	C	7.17	—	—	21.4 [9]
	25–1000*	—	—	—	—	105.8 [9]
SiO_2	300–1000	C	3.44	—	—	10.35 [30]

Note: T, tetragonal; C, cubic; O, orthorhombic. *Average thermal expansion coefficient in the given temperature range.

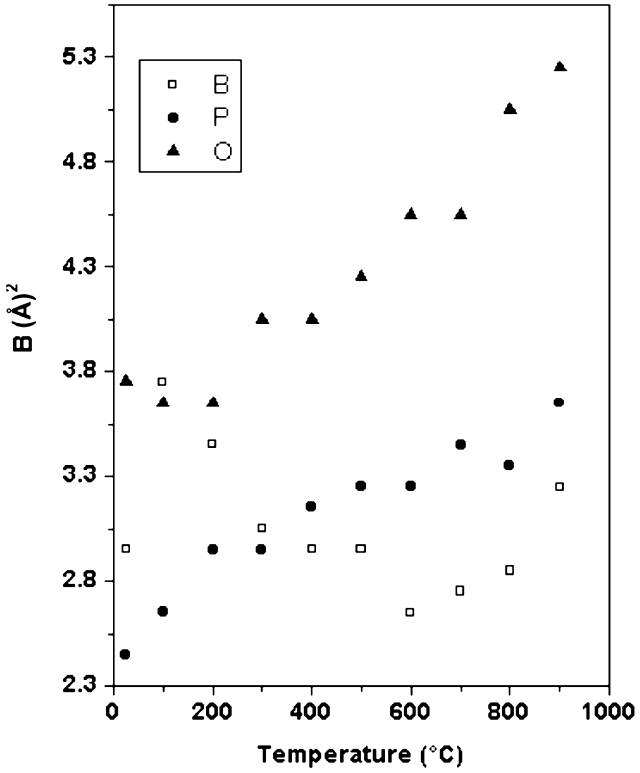

Fig. 7. Variation of isotropic thermal parameters of various atoms with temperature. Accuracy ± 1.5, ± 0.5 and $\pm 0.5\,\text{Å}^2$ for O, B and P atoms, respectively.

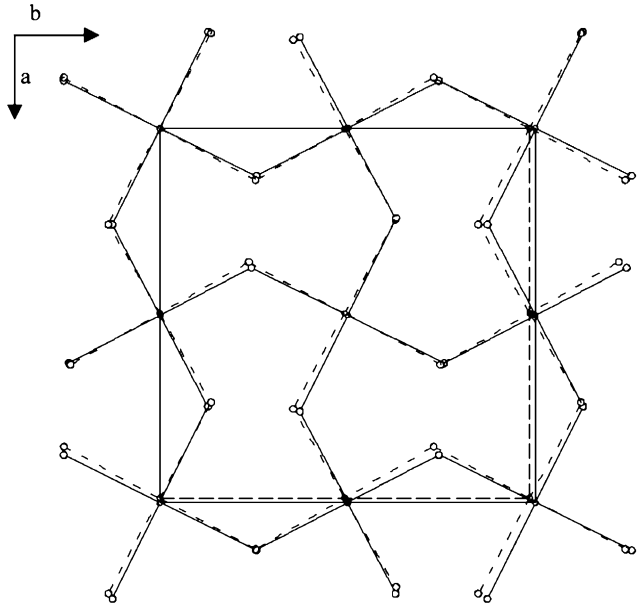

Fig. 8. Overlap of 0 0 1 projection of BPO_4 structures (broken line at 25°C and solid line at 900 °C). Symbols: small open circles (P), small close circles (B) and large open circles (O).

increase in P–O distance is only apparent and the actual bond should not show any deviation with temperature.

The arrangement of position coordinates of various atoms with increasing temperatures shows that the B–O–P angle increases with the increase in temperature, viz., 132.3(3)° (at 25 °C) to 135.8(4)° (at 900 °C). This increase in bond angle is reflected in the increase of average B–P distances (shortest separation) (Table 2 and Fig. 8), which resulted in an increase in the lattice parameters along *a*- and *b*-axis. A 0 0 1 projection of the structures at 25 and 900 °C is shown in Fig. 8. This figure indicates the relaxation of the *M*–O–P angle at 900 °C leading to an increase in the *a*- and *b*-axis. As seen from the Table 2 and Fig. 8, the increases in the distance between the non-bonded B and P atoms are significant. The typical coefficient of expansion in the non-bonded B–P distances is $9.0\times10^{-6}/°C$. The significant difference in the thermal expansion coefficient is a simple manifestation of this B⋯P separation and the angle between these separations.

A comparison of the crystal structure and thermal expansion coefficients of various cristobalite-type compounds indicates the inter-polyhedral angle has a significant influence on the volume thermal expansion coefficients (α_V). The variations of typical inter-polyhedral angle vs. α_V for several cristobalite-type compounds are shown in Fig. 9. It is observed that higher the inter-polyhedral angle smaller the volume thermal expansion coefficient. This can be explained due to the thermal vibration of the bridging oxygen atoms (which increase with increasing temperature), and hence the bent angle tends to dilate to accommodate the vibrating oxygen atom. This concept has been used to explain the negative thermal expansion behavior of several framework compounds ([1,6] and the references cited therein). By comparing the thermal expansion behavior of several compound, Evans et al. [2,3] have concluded that the typical bond angles between 150° and 174° tend to bend more leading to negative thermal expansion, whereas the values lower than 150° causes dilation of the *M*–O–P bond angle leading to positive thermal expansion coefficient. Since, the B–O–P bond angle has a significantly lower value, an appreciable positive thermal expansion is observed.

The high-temperature behavior of several quartz and cristobalite silica analogs ABO_4 (where $A=Al^{3+}$, Ga^{3+}, Fe^{3+} and $B=P^{5+}$, As^{5+}) and AO_2 ($A=Si^{4+}$ and Ge^{4+}) have been reported in the literature [8,28–36]. In all these studies, a greater dependency of inter-polyhedral angles with temperature has been reported. The symmetry changes in low-quartz to high-quartz or the low-cristobalite to high-cristobalite transformations as well as the typical thermal expansion behavior are closely related to change in inter-polyhedral angle. We have restricted this particular study to the description of the cristobalite-type compounds only. The cristobalite-type phase is observed for both AO_2- and ABO_4-type

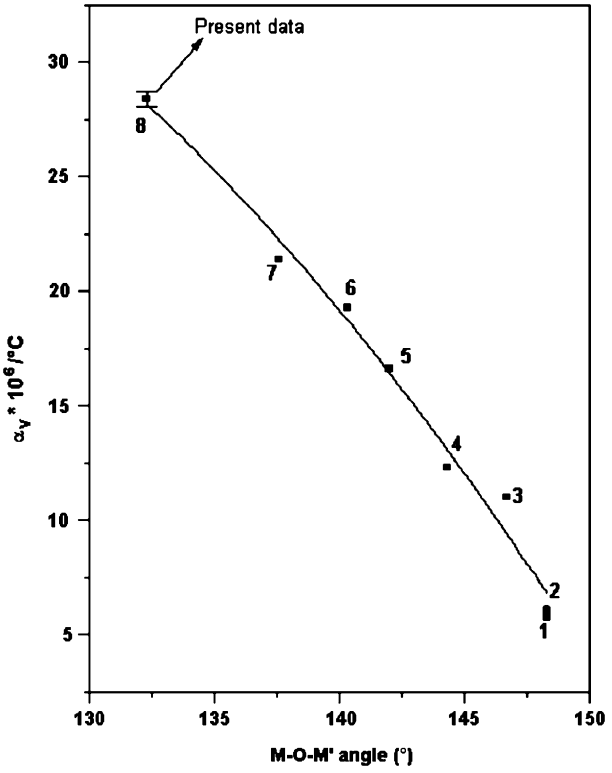

Fig. 9. Variation thermal expansion coefficients with inter-polyhedral angle α_V (/°C) = −191.32 + 4.33[θ] − 0.02[θ]^2. The values of angles are taken as: (1) $AlPO_4$ (at 300 °C) [9], (2) AlPO4 (at 300 °C) [32], (3) SiO_2 (at 300 °C) [32], (4) $Al_{0.8}Ga_{0.2}PO_4$ (at 300 °C) [9], (5) $Al_{0.5}Ga_{0.5}PO_4$ (at 400 °C) [9], (6) $Al_{0.2}Ga_{0.8}PO_4$ (at 600 °C) [9], (7) GaPO4 (at 700 °C) [9] and (8) BPO_4 (at 25 °C) (present data).

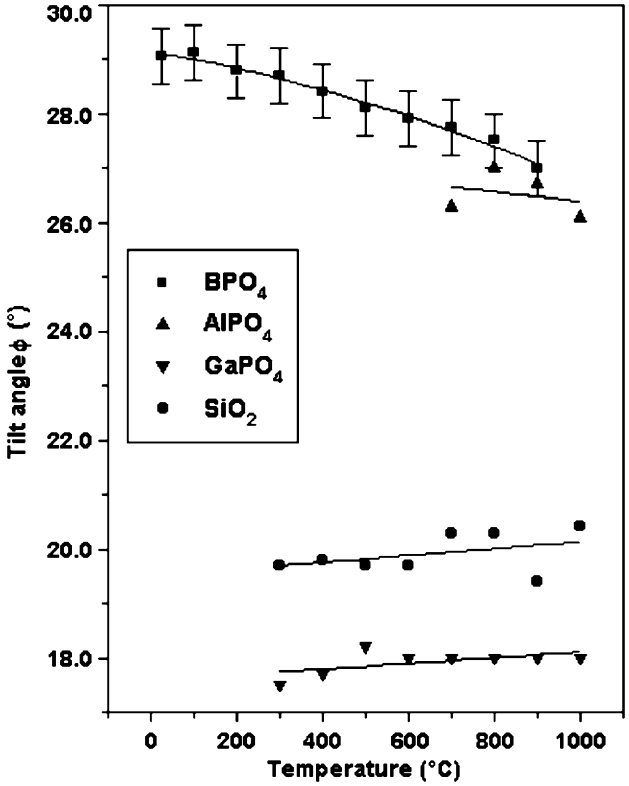

Fig. 10. Variation of tilt angle with temperature, $AlPO_4$ and $GaPO_4$ were taken from Ref. [9] and SiO_2 data were taken from Ref. [32].

compounds at higher temperature. But, all the phases can be stabilized at ambient temperature by suitable heat treatment. The stable low-cristobalite-type phases for SiO_2, $AlPO_4$/$GaPO_4$, etc. have tetragonal ($P4_12_12$) and orthorhombic ($C222_1$) lattice [30–32]. At higher temperature they undergo displacive transition to cubic lattice with space groups *Fd*3*m* and *F*-43*m*, respectively. The BPO_4, $BAsO_4$, $BeSO_4$, etc. crystallizes only in high-cristobalite-type structure, with space group *I*-4 [16]. All these structures are derived from the ideal C9 structure by rotating the tetrahedra around the *c*-axis, i.e., –4 axis. For a better comparison of the high-cristobalite-type SiO_2 (*Fd*3*m*), ideal C9 structure and the present BPO_4 structure, the space group *I*-42*d* for SiO_2 and C9 structure ($c/a = 1.414$) are used. In ideal C9 structure, the O positions are: 8*d* (*x*, 0.25, 0.125) for $x = 0.0$, whereas those in the real high-cristobalite-type SiO_2 are: 8*d* (0.91, 0.25, 0.125). The symmetry is further lowered to *I*-4 in BPO_4 due to the ordering of B and P atoms in the lattice and in the present investigation the observed oxygen positions in the unit cell are: 8*g* (*xyz*: 0.1389(10), 0.2589(11), 0.1275(5)). The tilting of tetrahedra about the *c*-axis is reflected from the shift in the *x*-parameter from the ideal value. A comparison of the *y* and *z* values of the oxygen positions at various temperatures indicates no significant difference and also they are marginally different from the ideal values. The insignificant variation of the *z* coordinates is reflected by the lower expansion of the *c*-axis. The relations of the tilt angle to the *x*-parameter as well as inter-polyhedral angles for the cristobalite-type phases are explained by O'Keeffe and Hyde [16].

The typical tilt angles at each temperature are calculated for this structure using the relation $\phi = \tan^{-1}(4x)$ [16], where $x = x$ value of the position coordinates of oxygen atoms. The tilting angle (ϕ) for BPO_4 at room temperature (25 °C) is 29.06°, which agrees well with the value reported (29.3° at 0.1 MPa) by Haines et al. [21] and (29.0° at RT) by Schulze [12]. The similar tilt angles at higher temperatures are also calculated and included in Table 2. It is observed from the Table 2 that the tilt angle gradually decreases from the maximum value of 29.1–27.0° as temperature increases from 25 to 900 °C, which is reflected in Fig. 10. The variation of tilt angle of the BPO_4 with temperature and the calculated tilt angles for other related reported cristobalite structures are also presented in Fig. 10. It shows that the tilt angle for BPO_4 decreases appreciably with temperature, whereas for other analogs, either an insignificant variation or a subtle positive increase is observed. This kind of tilting

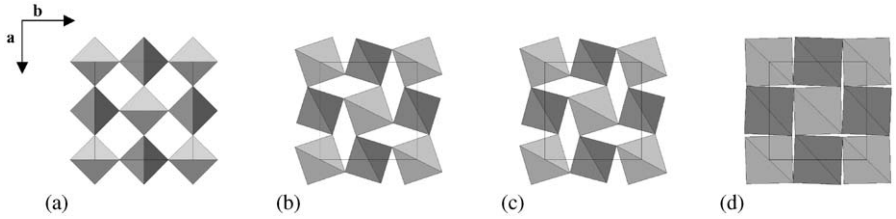

Fig. 11. Variation of cristobalite structures with tilt angle (ϕ) (only 0 0 1 projection is given): (a) C9 structure ($c/a=1.414$, $\phi=0$) [16], (b) BPO_4 at 900 °C ($c/a=1.514$, $\phi=27°$) (present data), (c) BPO_4 at 25 °C ($c/a=1.529$, $\phi=29°$) (present data) and (d) BPO_4 at 50 GPa ($c/a=1.954$, $\phi=43°$) [21].

of polyhedra in quartz-type structure was recently used to explain the thermal expansion of several quartz-type framework structures [34,35]. A comparison of the present variation of structure with temperature with the reported structural variation with pressure in the case of BPO_4 [21] again shows a close but inverse relation. On application of pressure the x-parameter of oxygen atom increases and thus the tilt angle also increases. The tilt angle increases gradually from the normal 29.3° (at 0.1 MPa) to 43.3° (at 50 GPa) for BPO_4 [21]. Thus, the tilt angle increases with the pressure giving a densely packed structure, whereas in the present investigation an opposite effect is observed with temperature. The variation of structure with tilt angle is shown in Fig. 11. It is obvious that the C9 structure, i.e., zero tilt angle (Fig. 10a), shows maximum separation between B and P atoms. Another extreme is the collapsed cristobalite ($\phi=43.3°$) structure of BPO_4 [16] (Fig. 10d). The two representative tilts 27° (at 900 °C) and 29° (at 25 °C) of BPO_4 appears in between this series (Fig. 10b and c). This order of tilt has a significant effect on the a- and b-axis and hence resulted in a significant increase in the c/a from the ideal value of 1.41–1.95 as the tilt changes from 0° to 43°. Consequently, this variation of the tilt angle with pressure or temperature is related with the compressibility or thermal expansion of such silica analog compounds.

4. Conclusion

From this study, it was observed that BPO_4 has a strong anisotropic lattice thermal expansion. The axial thermal expansion coefficients of this compound are $\alpha_a=12.9\times10^{-6}/°C$ and $\alpha_c=2.1\times10^{-6}/°C$ in the temperature range of 25–900 °C. The anisotropic thermal expansion behavior is due to the cooperative titling of the BO_4 and PO_4 tetrahedra in the unit cell around the –4 axis parallel to c-axis. The typical volume thermal expansion coefficient for this is found to be about $28.2\times10^{-6}/°C$ in this temperature range. The volume thermal expansion coefficient of cristobalite-type phases is strongly influenced by the M–O–P bond angles.

Acknowledgment

The authors thank Dr. N.M. Gupta, Head, Applied Chemistry Division, BARC, for his keen interest in this work.

References

[1] J.S.O. Evans, T.A. Mary, T. Vogt, M.A. Subramanian, A.W. Sleight, Chem. Mater. 8 (1996) 2809.
[2] J.S.O. Evans, T.A. Mary, A.W. Sleight, J. Solid State Chem. 137 (1998) 148.
[3] J.S.O. Evans, T.A. Mary, A.W. Sleight, J. Solid State Chem. 133 (1997) 580.
[4] T.G. Amos, A.W. Sleight, J. Solid State Chem. 160 (2001) 230.
[5] P.M. Forster, A.W. Sleight, Int. J. Inorg. Mater. 1 (1999) 123.
[6] J.Z. Tao, A.W. Sleight, J. Solid State Chem. 173 (2003) 45.
[7] N. Khosrovani, A.W. Sleight, Int. J. Inorg. Mater. 1 (1999) 3.
[8] J.S.O. Evans, T.A. Mary, A.W. Sleight, Physica B 241–243 (1998) 311.
[9] S.N. Achary, O.D. Jayakumar, A.K. Tyagi, S.K. Kulshreshtha, J. Solid State Chem. 176 (2003) 37.
[10] A.K.A. Pryde, K.D. Hammonds, M.T. Dove, V. Heine, J.D. Gale, M.C. Warren, J. Phys.: Condens. Matter 8 (1996) 10973.
[11] R. Mittal, S.L. Chaplot, H. Schober, T.A. Mary, Phys. Rev. Lett. 86 (2001) 4692.
[12] G.E.R. Schulze, Z. Phys. Chem. 24 (1934) 215.
[13] J.D. Mackenzie, W.L. Roth, R.H. Wentorf, Acta Cryst. 12 (1959) 79.
[14] J. Haines, C. Chateau, J.M. Leger, R. Marchand, Ann. Chim. Sci. Mater. 26 (2001) 209.
[15] R.W.G. Wyckoff, Am. J. Sci. 209 (1925) 448.
[16] M. O'Keeffe, B.G. Hyde, Acta Cryst. B 32 (1976) 2923.
[17] J.S.O. Evans, Z. Hu, J.D. Jorgenson, D.N. Argyriou, S. Short, A.W. Sleight, Science 275 (1997) 61.
[18] S.N. Achary, G.D. Mukherjee, A.K. Tyagi, B.K. Godwal, Phys. Rev. B. 66 (2002) 184106.
[19] A.K. Tyagi, S.N. Achary, M.D. Mathews, J. Alloys Compounds 339 (2002) 207.
[20] A.W. Sleight, L.H. Bixner, J. Solid State Chem. 7 (1973) 172.
[21] J. Haines, C. Chateau, J.M. Leger, C. Bogicevic, S. Hull, D.D. Klug, J.S. Tse, Phys. Rev. Lett. 91 (2003) 015503.
[22] J. Rodriguez-Caravajal, Sattelite meeting on powder diffraction, 15th Conference of the International Union of Crystals, Toulouse, France, 1990, p. 127.
[23] R.M. Hazen, C.T. Prewitt, Am. Mineral. 62 (1977) 309.
[24] V. Schomaker, K.N. Trueblood, Acta Cryst. B 24 (1968) 63.
[25] D.W. Cruickshank, Acta Cryst. 9 (1956) 757.
[26] M.G. Tucker, M.T. Dove, D.A. Keen, J. Phys.: Condens. Matter 12 (2000) L425.

[27] H. Grimm, B. Dorner, J. Phys. Chem. Solids 36 (1975) 407.
[28] K. Maraoka, K. Kihara, Phys. Chem. Miner. 24 (1997) 243.
[29] P. Worsch, B. Koppenlhuber-Bitschnau, F.A. Mautner, P.W. Krempl, W. Wallnofer, Mater. Sci. Forum 278–281 (1998) 600.
[30] H.N. Ng, C. Calvo, Can. J. Phys. 55 (1977) 677.
[31] P. Worsch, B. Koppenlhuber-Bitschnau, F.A. Mautner, P.W. Krempl, W. Wallnofer, P. Doppler, J. Gautsch, Mater. Sci. Forum 312–324 (2000) 914.
[32] A.F. Wright, A.J. Leadbetter, Philos. Mag. 31 (1975) 1391.
[33] D.M. Hatch, S. Ghose, J.L. Bjorkstam, Phys. Chem. Miner. 21 (1994) 67.
[34] E. Philippot, P. Armand, P. Yot, O. Cambon, A. Goiffon, G.J. McIntyre, P. Bordet, J. Solid State Chem. 146 (1999) 114.
[35] J. Haines, O. Cambon, E. Philippot, L. Chapon, S. Hull, J. Solid state Chem. 166 (2002) 434.
[36] J.M. Leger, J. Haines, C. Chateau, G. Bocquillon, M.W. Schmidt, S. Hull, F. Gorelli, A. Lesauze, R. Marchand, Phys. Chem. Miner. 28 (2001) 388.